



CHORUS

This is the accepted manuscript made available via CHORUS. The article has been published as:

Optical and photoemission investigation of structural and magnetic transitions in the iron-based superconductor $\text{Sr}_{0.67}\text{Na}_{0.33}\text{Fe}_2\text{As}_2$

R. Yang, J. W. Huang, N. Zaki, I. Pletikosić, Y. M. Dai, H. Xiao, T. Valla, P. D. Johnson, X. J. Zhou, X. G. Qiu, and C. C. Homes

Phys. Rev. B **100**, 235132 — Published 20 December 2019

DOI: [10.1103/PhysRevB.100.235132](https://doi.org/10.1103/PhysRevB.100.235132)

Optical and photoemission investigation of structural and magnetic transitions in the iron-based superconductor $\text{Sr}_{0.67}\text{Na}_{0.33}\text{Fe}_2\text{As}_2$

R. Yang,^{1,2,3,*} J. W. Huang,^{2,3} N. Zaki,¹ I. Pletikosić,^{1,4} Y. M. Dai,⁵ H. Xiao,⁶
T. Valla,¹ P. D. Johnson,¹ X. J. Zhou,^{2,3,7,8} X. G. Qiu,^{2,3,7,†} and C. C. Homes^{1,‡}

¹*Condensed Matter Physics and Materials Science Division,
Brookhaven National Laboratory, Upton, New York 11973, USA*

²*Beijing National Laboratory for Condensed Matter Physics,
Institute of Physics, Chinese Academy of Sciences, Beijing 100190, China*

³*School of Physical Sciences, University of Chinese Academy of Sciences, Beijing 100049, China*

⁴*Department of Physics, Princeton University, Princeton, NJ 08544, USA*

⁵*Center for Superconducting Physics and Materials,
National Laboratory of Solid State Microstructures and Department of Physics, Nanjing University, Nanjing 210093, China*

⁶*Center for High Pressure Science and Technology Advanced Research, Beijing 100094, China*

⁷*Songshan Lake Materials Laboratory, Dongguan 523808, China*

⁸*Beijing Academy of Quantum Information Science, Beijing 100193, China*

(Dated: December 6, 2019; version 5.2)

We report the temperature dependent optical conductivity and angle-resolved photoemission spectroscopy (ARPES) studies of the multiband iron-based superconductor $\text{Sr}_{0.67}\text{Na}_{0.33}\text{Fe}_2\text{As}_2$. Measurements were made in the high-temperature tetragonal paramagnetic phase; below the structural and magnetic transitions at $T_N \simeq 125$ K in the orthorhombic spin-density-wave (SDW)-like phase, and $T_r \simeq 42$ K in the reentrant tetragonal double- \mathbf{Q} magnetic phase where both charge and SDW order exist; and below the superconducting transition at $T_c \simeq 10$ K. The free-carrier component in the optical conductivity is described by two Drude contributions; one strong and broad, the other weak and narrow. The broad Drude component decreases dramatically below T_N and T_r , with much of its strength being transferred to a bound excitation in the mid-infrared, while the narrow Drude component shows no anomalies at either of the transitions, actually increasing in strength at low temperature while narrowing dramatically. The behavior of an infrared-active mode suggests zone-folding below T_r . Below T_c the dramatic decrease in the low-frequency optical conductivity signals the formation of a superconducting energy gap. ARPES reveals hole-like bands at the center of the Brillouin zone (BZ), with both electron- and hole-like bands at the corners. Below T_N , the hole pockets at the center of the BZ decrease in size, consistent with the behavior of the broad Drude component; while below T_r the electron-like bands shift and split, giving rise to a low-energy excitation in the optical conductivity at $\simeq 20$ meV. The C_2 and C_4 magnetic states, with resulting spin-density-wave and charge-SDW order, respectively, lead to a significant reconstruction of the Fermi surface that has profound implications for the transport originating from the electron and hole pockets, but appears to have relatively little impact on the superconductivity in this material.

PACS numbers: 72.15.-v, 74.70.-b, 78.20.-e

I. INTRODUCTION

The discovery of iron-based superconductors prompted an intensive investigation in the hope of identifying new compounds with high superconducting critical temperatures (T_c 's) [1–4]. In many of the iron-based materials, superconductivity emerges with the suppression of anti-ferromagnetic (AFM) order, suggesting that the pairing mechanism is related to the magnetism. Indeed, the iron-based materials display a variety of magnetically-ordered ground states [5–9] that may either compete with or foster the emergence of superconductivity.

One class of materials, $A\text{eFe}_2\text{As}_2$, where $A\text{e} = \text{Ba}, \text{Ca}$

or Sr (the so-called “122” materials), is particularly useful as superconductivity may be induced through a variety of chemical substitutions [10–20], as well as through the application of pressure [21–24]. The phase diagram of $\text{Sr}_{1-x}\text{Na}_x\text{Fe}_2\text{As}_2$ has a number of interesting features. At room temperature, the parent compound SrFe_2As_2 is a paramagnetic metal with a tetragonal ($I4/mmm$) structure. The resistivity in the iron-arsenic planes decreases with temperature until it drops anomalously as the material undergoes a magnetic transition at $T_N \simeq 195$ K to a spin-density-wave (SDW)-like AFM ground state that is also accompanied by a structural transition to an orthorhombic ($Fmmm$) phase [25–30]. The crystals are heavily twinned in the orthorhombic phase; however, the application of uniaxial stress along the (110) direction of the tetragonal unit cell results in a nearly twin-free sample [31, 32]. The magnetic order may be described as AFM stripes, where the iron spins are aligned antiferromagnetically along the a axis and ferromagnetically along

* Present address: Laboratorium für Festkörperphysik, ETH Zürich, CH-8093 Zürich, Switzerland

† xgqiu@iphy.ac.cn

‡ homes@bnl.gov

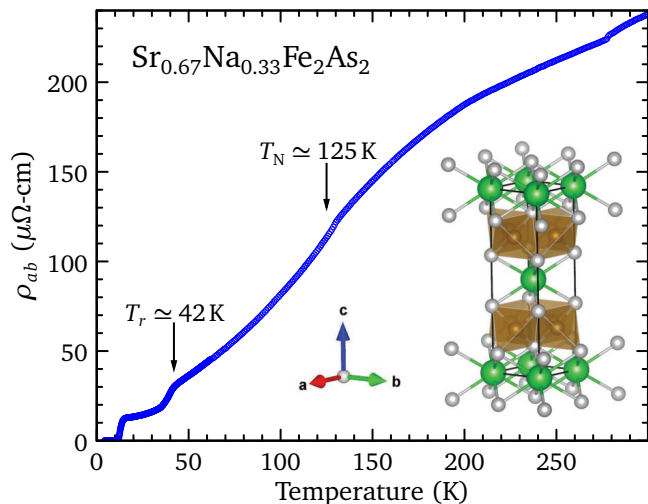


Figure 1. The temperature dependence of the in-plane resistivity for $\text{Sr}_{0.67}\text{Na}_{0.33}\text{Fe}_2\text{As}_2$ with inflection points at $T_N \simeq 125$ K and $T_r \simeq 42$ K; the resistivity at room temperature has been adjusted to match the optical conductivity in the zero-frequency limit. Inset: The generic unit cell in the high-temperature tetragonal phase for the 122 materials.

the b axis [33, 34]; this is also referred to as the magnetic C_2 phase due to its twofold rotation symmetry. As the sodium content increases, the magnetic and structural transition temperatures decrease until both disappear at $x \simeq 0.48$; superconductivity appears well before this point at $x \simeq 0.2$, and reaches a maximum of $T_c \simeq 37$ K for $x \simeq 0.5 - 0.6$. Between $0.29 < x < 0.42$, an additional magnetic and structural transition occurs below T_N at T_r ; the tetragonal ($I4/mmm$) phase reemerges, forming a dome which lies completely within the AFM region. This phase appears to be a common element in the hole-doped 122 materials [35–45]; however, in $\text{Sr}_{1-x}\text{Na}_x\text{Fe}_2\text{As}_2$ the dome is more robust and occurs over a wider doping range at temperatures up to $T_r \simeq 65$ K [39, 40], which is higher than has been observed in other compounds. This magnetic order is described as the collinear superposition of two itinerant SDW's with nesting wavevector \mathbf{Q} , leading to a double- \mathbf{Q} SDW [44, 45] in which half the iron sites are nonmagnetic, and half have twice the moment measured in the orthorhombic AFM phase, oriented along the c axis [46, 47]; this is referred to as the magnetic C_4 phase because of its fourfold rotational invariance. This magnetic state is accompanied by a charge-density wave (CDW) with the charge coupling to the square of the magnetization, resulting in a charge-SDW (CSDW) [48].

In this work, the complex optical properties and angle-resolved photoemission spectroscopy (ARPES), of $\text{Sr}_{0.67}\text{Na}_{0.33}\text{Fe}_2\text{As}_2$ have been investigated in the high-temperature tetragonal phase, as well as the magnetic C_2 and C_4 phases. The value of $x \simeq 0.33$ used in the current study is slightly below the optimal value of $x \simeq 0.37$ that bisects the C_4 dome in the $\text{Sr}_{1-x}\text{Na}_x\text{Fe}_2\text{As}_2$ phase diagram [39]. Based on transport studies, $T_N \simeq 125$ K,

$T_r \simeq 42$ K, and $T_c \simeq 10$ K. In the high temperature tetragonal paramagnetic state, the optical response of the free-carriers is described by two Drude terms (Sec. IIIA); one strong and broad (large scattering rate), and the other weak and narrower (smaller scattering rate); as the temperature is reduced, the strength of the Drude terms show relatively little temperature dependence, while the scattering rates slowly decrease. Below T_N , the Fermi surface reconstruction driven by the structural and magnetic transitions causes both the strength and the scattering rate for the broad Drude term to decrease dramatically; the missing spectral weight (the area under the conductivity curve) associated with the free carriers is transferred to a peak that emerges in the mid-infrared. The narrow Drude term actually increases slightly in strength below T_N while narrowing. Below T_r , in the magnetic C_4 phase, the broad Drude term again narrows and decreases in strength; while the strength of the narrow term does not appear to change, its scattering rate decreases dramatically. Based on the behavior of an infrared-active lattice mode, the presence of CSDW order likely results in the formation of a supercell resulting in zone folding, leading to a further reconstruction of the Fermi surface; while spectral weight is again transferred from the broad Drude to the midinfrared peak, a new low-energy peak emerges at $\simeq 20$ meV. Below T_c , there is a dramatic decrease in the low-frequency conductivity, signalling the formation of a superconducting energy gap. ARPES reveals several large hole pockets at the center of the Brillouin zone above T_N , one of which shifts below the Fermi level below T_N in the C_2 magnetic phase, a trend which continues below T_r , suggesting that these bands may be related to the broad Drude response. At the corners of the Brillouin zone, there are both hole- and electron-like bands. Below T_N and T_r , several of these bands appear to split and shift, but it is not clear if there are any significant changes to the size of the associated Fermi surfaces, suggesting that some of these carriers may be related to the narrow Drude term; below T_r the band splitting is likely responsible for the emergence of the low-energy peak. The structural and magnetic transitions from which the C_2 (SDW) and C_4 (double- \mathbf{Q} SDW) phases emerge result in a Fermi surface reconstruction that has profound effects on the optical conductivity and electronic structure; however, the superfluid stiffness appears to be more or less unaffected by the CSDW order.

II. EXPERIMENT

High-quality single crystals of $\text{Sr}_{0.67}\text{Na}_{0.33}\text{Fe}_2\text{As}_2$ with good cleavage planes (001) were synthesized using a self-flux technique [39, 49]. The temperature dependence of the in-plane resistivity, shown in Fig. 1, was measured using a standard four-probe configuration using a Quantum Design physical property measurement system; the unit cell for the high-temperature tetragonal phase is

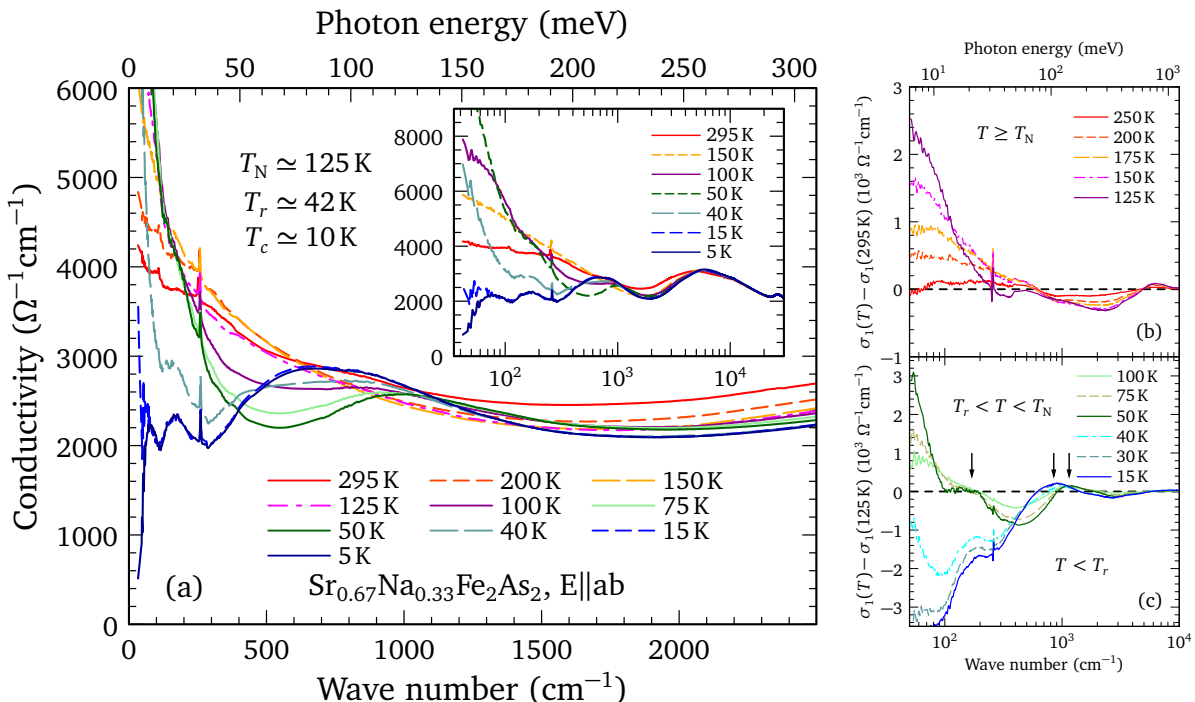


Figure 2. (a) The temperature dependence of the real part of the optical conductivity of $\text{Sr}_{0.67}\text{Na}_{0.33}\text{Fe}_2\text{As}_2$ in the infrared region for light polarized in the Fe–As planes. Inset: the conductivity over a wide spectral range at several temperatures. (b) The $\sigma_1(\omega, T) - \sigma_1(\omega, 295\text{K})$ difference plot for $T \geq T_N$ over a wide spectral range showing the narrowing of the free-carrier response and the transfer of spectral weight from high to low frequency. (c) The $\sigma_1(\omega, T) - \sigma_1(\omega, 125\text{K})$ difference plot. In the $T_r < T < T_N$ region the free-carrier response continues to narrow and a peak emerges in the mid-infrared region; for $T < T_r$, the low-frequency conductivity is further suppressed, the mid-infrared peak shifts to low energy, and a prominent peak is observed at $\simeq 170\text{ cm}^{-1}$ (arrows).

shown in the inset. The resistivity decreases gradually with temperature, showing a weak inflection point at $T_N \simeq 125\text{ K}$ with a more pronounced decrease in the resistivity at $T_r \simeq 42\text{ K}$; the resistivity goes to zero below the superconducting transition at $T_c \simeq 10\text{ K}$. The reflectance from freshly-cleaved surfaces has been measured at a near-normal angle of incidence over a wide temperature ($\simeq 5$ to 300 K) and frequency range ($\simeq 2\text{ meV}$ to about 5 eV) with Bruker IFS 113v and Vertex 80v Fourier transform spectrometers for light polarized in the a - b planes using an *in situ* evaporation technique [50]. The complex optical properties have been determined from a Kramers-Kronig analysis of the reflectivity. The reflectivity is shown in supplementary Fig. S1; the details of the Kramers-Kronig analysis are described in the Supplementary Material [51]. Temperature dependent ARPES measurements have been performed to track the evolution of the electron and hole pockets in the various phases. Measurements at BNL, which focused on the electronic structure near the center of the Brillouin zone, were performed using 21.2 eV light from a monochromator-filtered He I source (Omicron VUV5k) and a Scienta SES-R4000 electron spectrometer; emitted electrons were collected along the direction perpendicular to the light-surface mirror plane. Samples were cleaved

at low temperature and measured in an ultrahigh vacuum with a base pressure better than 5×10^{-10} mbar. Measurements at the National Laboratory for Superconductivity, Institute of Physics, Chinese Academy of Sciences, were performed using a 21.2 eV helium discharge lamp and a Scienta DA30L electron spectrometer. The latter's overall energy resolution was 10 meV for Fermi surface mapping and 4 meV for the cuts; the angular resolution was $\sim 0.1^\circ$. All the samples were cleaved at low temperature and measured in an ultrahigh vacuum with a base pressure better than 5×10^{-11} mbar. Note that because uniaxial strain is not applied to the samples below T_N , they will be heavily twinned, thus the optical and ARPES results represent an average of the a and b axis response in the magnetic C_2 phase.

III. RESULTS AND DISCUSSION

A. Optical properties

The temperature dependence of the real part of the in-plane optical conductivity [$\sigma_1(\omega)$] of $\text{Sr}_{0.67}\text{Na}_{0.33}\text{Fe}_2\text{As}_2$ is shown in the infrared region in Fig. 2(a) (an additional plot of the optical conductivity is shown in supplement-

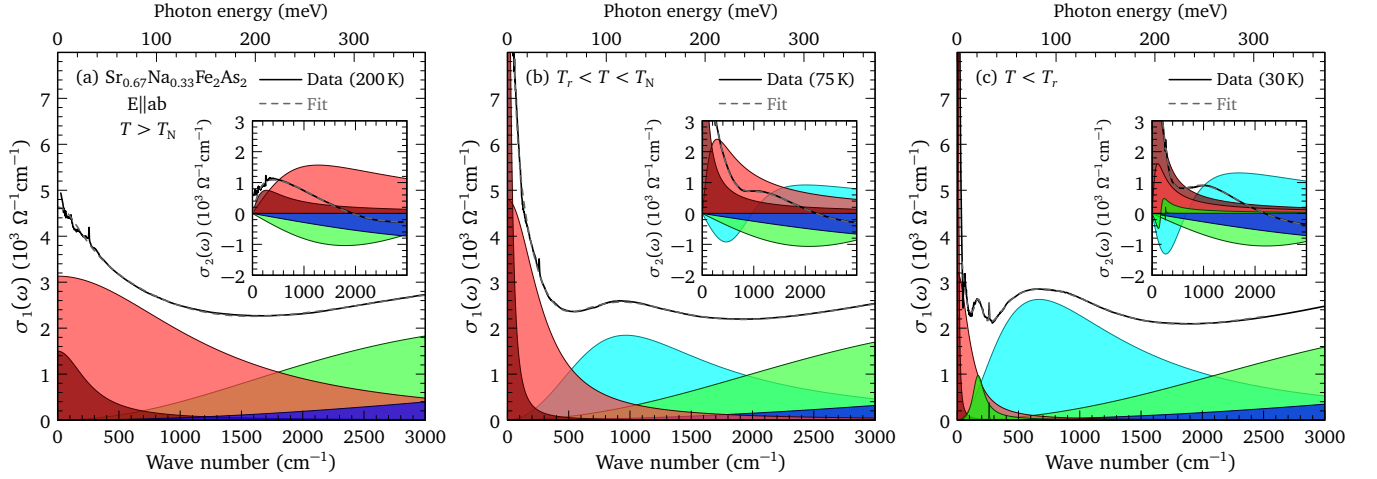


Figure 3. The Drude-Lorentz model fits to the real and imaginary (inset) parts of the in-plane optical conductivity of $\text{Sr}_{0.67}\text{Na}_{0.33}\text{Fe}_2\text{As}_2$ decomposed into the narrow (D1) and broad (D2) Drude components, as well as several bound excitations (a) above T_N at 200 K, (b) below T_N at 75 K showing the narrowing of the Drude features and the emergence of a peak at $\simeq 950\text{cm}^{-1}$, and (c) below T_r at 30 K, showing further narrowing and peaks at $\simeq 170$ and 700cm^{-1} .

183 tary Fig. S2). The character of the conductivity changes
184 dramatically through the structural and magnetic transi-
185 tions, which can be characterized by four distinct regions:
186 (i) $T > T_N$; (ii) $T_r < T < T_N$; (iii) $T < T_r$, and below the
187 superconducting transition (iv) $T < T_c$. The changes to
188 the nature of the conductivity are shown as the difference
189 plots $\sigma_1(\omega, T) - \sigma_1(\omega, 295\text{K})$, and $\sigma_1(\omega, T) - \sigma_1(\omega, 125\text{K})$,
190 shown in Figs. 2(b) and 2(c), respectively.

191 At room temperature, the free-carrier response appears
192 Drude-like (a Lorentzian centered at zero frequency with
193 a scattering rate defined as the full width at half maxi-
194 mum), giving way to a flat response at higher frequen-
195 cies, until the first interband transitions are encountered
196 at about 1 eV. As the temperature is reduced, the scat-
197 tering rate decreases and there is a slight reduction of
198 the conductivity in the mid-infrared region as spectral
199 weight is transferred from high to low frequency, which
200 leads to an increase at low frequency and a decrease at
201 high frequency in the difference spectra in Fig. 2(b). Be-
202 low T_N in the C_2 phase, the free-carrier response narrows
203 dramatically and a peak-like structure emerges at about
204 950cm^{-1} , somewhat lower than a similar feature that
205 was observed below T_N at $\simeq 1400\text{cm}^{-1}$ in the parent
206 compound SrFe_2As_2 [52]. This is illustrated by the upper
207 three curves in Fig. 2(c) that show the continuing increase
208 in the low-frequency conductivity, as well as the emer-
209 gence of a peak in the mid-infrared region. Interestingly,
210 below $\simeq 75\text{K}$, a low-energy peak at $\simeq 170\text{cm}^{-1}$ begins to
211 emerge. This behavior continues until $T \leq T_r$, at which
212 point the Drude-like response becomes extremely narrow
213 in the C_4 phase, illustrated by the dramatic suppression
214 of the low-frequency conductivity in the difference plot
215 in Fig. 2(c), leaving clearly identifiable peaks at $\simeq 170$
216 and 700cm^{-1} . Below $T_c \simeq 10\text{K}$, there is a depletion of
217 the low-frequency conductivity with the emergence of a
218 shoulder-like structure around 70cm^{-1} that signals the

219 formation of a superconducting energy gap (supplemen-
220 tary Fig. S2).

221 The sharp feature observed in the conductivity at
222 $\simeq 260\text{cm}^{-1}$ is attributed to a normally infrared-active
223 lattice vibration in the iron-arsenic planes; while this
224 mode increases in frequency with decreasing tempera-
225 ture, it does not display the anomalous increase in oscil-
226 lator strength below T_N that was observed in the parent
227 compound [53]. However, below T_r there is evidence for
228 a new satellite mode appearing at $\simeq 282\text{cm}^{-1}$ (supple-
229 mentary Fig. S3); a similar feature has also been observed
230 in the C_4 phase of $\text{Ba}_{1-x}\text{K}_x\text{Fe}_2\text{As}_2$ and is attributed to
231 Brillouin-zone folding due to the formation of a supercell
232 in the CSDW phase [54].

233 Previous optical studies of the iron-arsenic materials
234 recognized that these are multiband materials with hole
235 and electron pockets at the center and corners of the
236 Brillouin zone [55, 56]; a minimal description consists of
237 two electronic subsystems using the so-called two-Drude
238 model [57]. The complex dielectric function $\tilde{\epsilon} = \epsilon_1 + i\epsilon_2$
239 can be written as,

$$\tilde{\epsilon}(\omega) = \epsilon_\infty - \sum_{j=1}^2 \frac{\omega_{p,D;j}^2}{\omega^2 + i\omega/\tau_{D,j}} + \sum_k \frac{\Omega_k^2}{\omega_k^2 - \omega^2 - i\omega\gamma_k}, \quad (1)$$

240 where ϵ_∞ is the real part at high frequency. In the first
241 sum, $\omega_{p,D;j}^2 = 4\pi n_j e^2 / m_j^*$ and $1/\tau_{D,j}$ are the square of
242 the plasma frequency and scattering rate for the delo-
243 calized (Drude) carriers in the j th band, respectively,
244 and n_j and m_j^* are the carrier concentration and effec-
245 tive mass. In the second summation, ω_k , γ_k and Ω_k
246 are the position, width, and strength of the k th vibra-
247 tion or bound excitation. The complex conductivity is
248 $\tilde{\sigma}(\omega) = \sigma_1 + i\sigma_2 = -2\pi i\omega[\tilde{\epsilon}(\omega) - \epsilon_\infty]/Z_0$ (in units of
249 $\Omega^{-1}\text{cm}^{-1}$); $Z_0 \simeq 377\Omega$ is the impedance of free space.
250 The model is fit to the real and imaginary parts of the

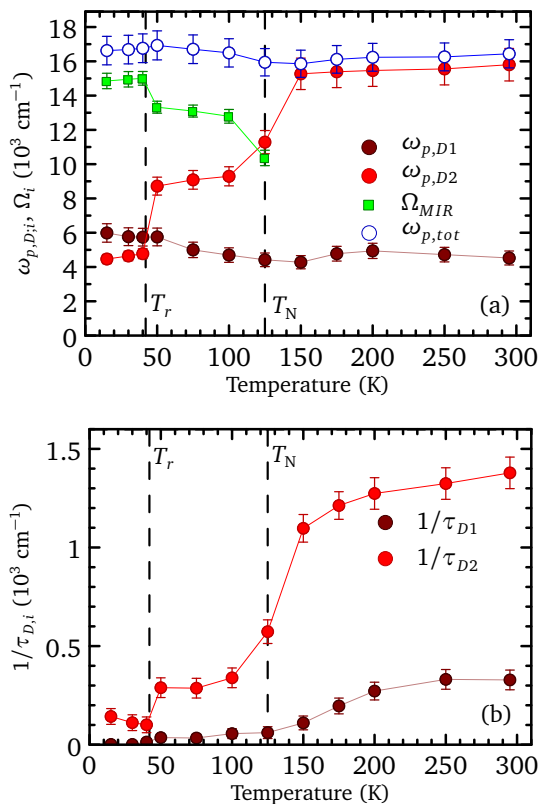


Figure 4. (a) The temperature dependence of the plasma frequencies of the narrow (D1) and broad (D2) Drude components, the oscillator strength of the mid-infrared peak (Ω_{MIR}), and the total when these three components are added in quadrature ($\omega_{p,tot}$), for Sr_{0.67}Na_{0.33}Fe₂As₂. (b) The temperature dependence of the scattering rates of the narrow and broad Drude components.

optical conductivity simultaneously using a non-linear least-squares technique. The results of the fits are shown in Figs. 3(a), 3(b), and 3(c) at 200 K ($T > T_N$), 75 K ($T_r < T < T_N$), and 30 K ($T < T_r$), respectively; the combined response has been decomposed into individual Drude and Lorentz components. In agreement with previous studies on the iron-based materials, the complex conductivity can be described by two Drude terms, one weak and narrow (D1), the other strong and broad (D2), as well as several Lorentzian oscillators. The temperature dependence of the plasma frequencies, the D1 and D2 components, as well as the strength of the mid-infrared (MIR) peak, are shown in Fig. 4(a); the temperature dependence of the scattering rates for the two Drude components is shown in Fig. 4(b).

1. $T > T_N$

At room temperature, the plasma frequencies for the narrow and broad Drude terms, $\omega_{p,D1} \simeq 4400 \text{ cm}^{-1}$ and $\omega_{p,D2} \simeq 15800 \text{ cm}^{-1}$, respectively, are slightly less

than those of the undoped parent compound SrFe₂As₂ ($\omega_{p,D1} \simeq 5200 \text{ cm}^{-1}$ and $\omega_{p,D2} \simeq 17700 \text{ cm}^{-1}$); however, the scattering rates of $1/\tau_{D1} \simeq 330 \text{ cm}^{-1}$ and $1/\tau_{D2} \simeq 1400 \text{ cm}^{-1}$ are noticeably lower than the values of $1/\tau_{D1} \simeq 470 \text{ cm}^{-1}$ and $1/\tau_{D2} \simeq 2330 \text{ cm}^{-1}$ observed in the undoped material [52]. This is somewhat surprising considering that in this material the layers in between the Fe-As sheets are disordered. While the plasma frequencies show little temperature dependence between room temperature and T_N , the scattering rates for both Drude components decrease with temperature, with the narrow Drude decreasing from about $1/\tau_{D1} \simeq 330$ to about 60 cm^{-1} , and the broad Drude decreasing from $1/\tau_{D2} \simeq 1400$ to about 1100 cm^{-1} just above T_N .

2. $T_r < T < T_N$

Below T_N in the magnetic C_2 phase, the plasma frequency for the narrow Drude increases slightly from $\omega_{p,D1} \simeq 4400$ to $\simeq 6000 \text{ cm}^{-1}$, while the scattering rate continues to decrease to $1/\tau_{D1} \simeq 40 \text{ cm}^{-1}$ just above T_r . The broad Drude displays much larger changes, with the plasma frequency decreasing from $\omega_{p,D2} \simeq 15800$ to 9000 cm^{-1} , which corresponds to a decrease in carrier concentration of nearly 65% ($\omega_p^2 \propto n/m^*$); the scattering rate also drops dramatically from $1/\tau_{D2} \simeq 1100 \text{ cm}^{-1}$ just above T_N to 300 cm^{-1} in the $T_r < T < T_N$ region. The dramatic loss of spectral weight of the broad Drude term is accompanied by the emergence of a new peak in the MIR region with position $\omega_{MIR} \simeq 950 \text{ cm}^{-1}$, width $\gamma_{MIR} \simeq 1550 \text{ cm}^{-1}$, and strength $\Omega_{MIR} \simeq 13000 \text{ cm}^{-1}$ [Fig. 3(b)]; the missing weight from the free carriers is transferred into this bound excitation, and accordingly the total spectral weight is defined as $\omega_{p,tot}^2 = \omega_{p,D1}^2 + \omega_{p,D2}^2 + \Omega_{MIR}^2$, is constant, as shown in Fig. 4(a). This behavior is similar to what was previously observed in the parent compound, and has been explained as the partial gapping of the pocket responsible for the broad Drude term due and the appearance of a low-energy interband transition [52, 58].

3. $T < T_r$

As the temperature is reduced the system undergoes a further magnetic and structural transition at $T_r \simeq 42 \text{ K}$ and enters the magnetic C_4 phase. Below T_r the plasma frequency for the narrow Drude term appears to actually increase slightly; however, this is accompanied by a dramatic collapse of $1/\tau_{D1} \simeq 40 \text{ cm}^{-1}$ just above T_r to a value of $\simeq 2 \text{ cm}^{-1}$ at 15 K; this is nearly an order of magnitude smaller than what is observed in the parent compound [52]. Consequently, the narrow Drude is no longer observable in $\sigma_1(\omega)$, leaving a relatively flat optical conductivity due to the broad Drude term and Lorentzian components; instead, its effects are determined from $\sigma_2(\omega)$ [shown in the inset of Fig. 3(c)].

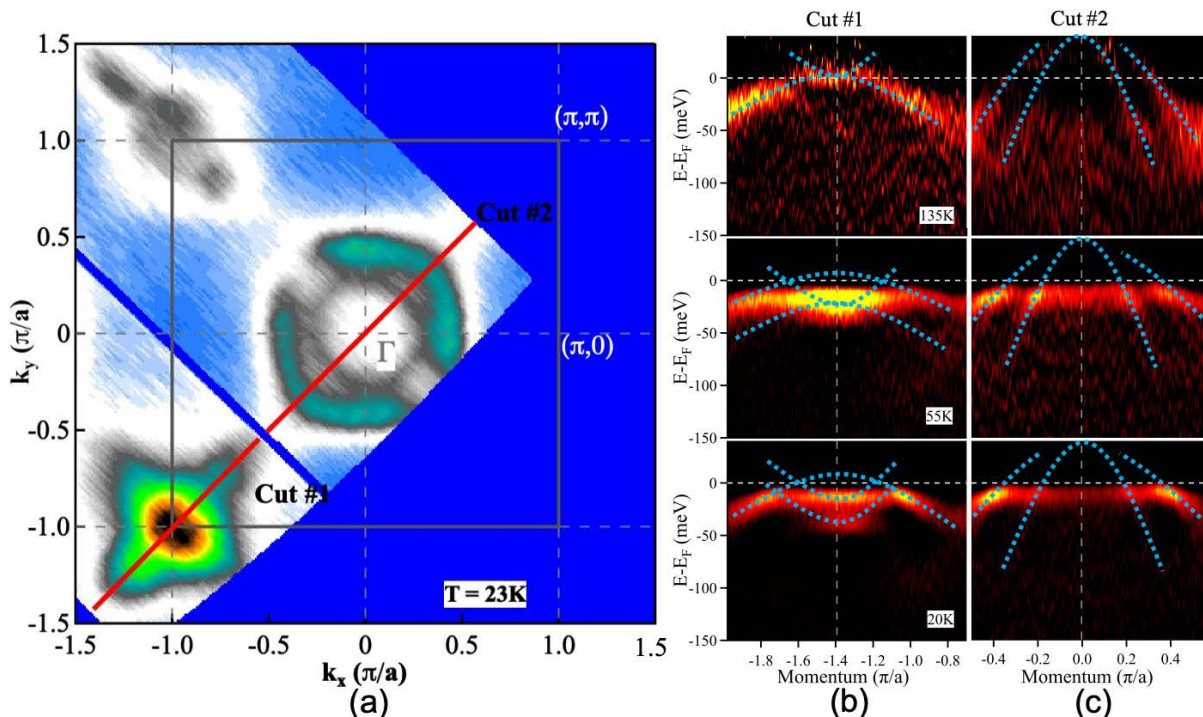


Figure 5. (a) Fermi surface mapping of $\text{Sr}_{0.67}\text{Na}_{0.33}\text{Fe}_2\text{As}_2$ in the C_4 magnetic phase at 23 K with the spectral weight integrated within a ± 10 meV energy window with respect to the Fermi level, showing the hole-like pockets at the center (Γ), and the electron-like pockets at the corner (M) of the Brillouin zone. Several different cuts are shown along the $\Gamma \rightarrow \text{M}$ path focus on the evolution of the hole and electron pockets. (b) The temperature dependence of the second derivative of the energy bands measured along the first cut around the M point at 135 K ($T > T_N$), 55 K ($T_r < T < T_N$), and 20 K ($T_c < T < T_r$). (c) The temperature dependence of the second derivative of the energy bands measured along the second cut around the Γ point at 135, 55, and 20 K. The dotted lines are drawn as a guide to the eye.

322 The plasma frequency of the broad Drude term contin-
 323 ues to decrease from $\omega_{p,D2} \simeq 9000$ to about 4200 cm^{-1}
 324 at 15 K, a further 80% reduction in the carrier con-
 325 centration associated with this pocket, and over 90%
 326 from the room temperature value; this is comparable to
 327 what was observed in the parent compound for $T \ll T_N$
 328 [52]. In addition, the scattering rate decreases from
 329 $1/\tau_{D2} \simeq 300 \text{ cm}^{-1}$ at T_r to $\simeq 120 \text{ cm}^{-1}$ at 15 K. At the
 330 same time, the peak at $\omega_{\text{MIR}} \simeq 950 \text{ cm}^{-1}$ shifts down to
 331 about $\simeq 650 \text{ cm}^{-1}$; while the width decreases slightly to
 332 $\gamma_{\text{MIR}} \simeq 1480 \text{ cm}^{-1}$, the strength of this feature increases
 333 to $\Omega_{\text{MIR}} \simeq 15400 \text{ cm}^{-1}$. However, $\omega_{p,\text{tot}}$ continues to
 334 be conserved, indicating that the loss of spectral weight
 335 associated with the free carriers in the broad Drude term
 336 has been transferred to this peak.

337 4. $T < T_c$

338 Below $T_c \simeq 10$ K there is a dramatic suppression of
 339 the low-frequency conductivity, signalling the formation
 340 of a superconducting energy gap [Fig. 2(a) and supple-
 341 mentary Fig. S2]. Although the low-frequency data is
 342 somewhat limited, a comparison of the optical conduc-

343 tivity for $T \gtrsim T_c$ and $T \ll T_c$ allows the superfluid den-
 344 sity, $\rho_s = \omega_{ps}^2$, where ω_{ps} is the superconducting plasma
 345 frequency, to be determined from the missing spec-
 346 tral weight, calculated using the Ferrell-Glover-Tinkham
 347 (FGT) sum rule [59, 60]. The FGT sum rule converges
 348 to $\omega_{ps} \simeq 5800 \pm 500 \text{ cm}^{-1}$, which corresponds to a super-
 349 conducting penetration depth of $\lambda \simeq 2700 \pm 300 \text{ \AA}$ at 5 K,
 350 comparable to the K-doped material [47]; however, be-
 351 cause the lowest temperature obtained was only $\simeq T_c/2$,
 352 it is almost certain that ω_{ps} is underestimated. From
 353 Fig. 2(a) and supplementary Fig. S2, the characteristic
 354 energy scale for the superconducting energy gap is about
 355 $2\Delta \simeq 50 \text{ cm}^{-1}$. In the narrow Drude band, $1/\tau_{D1} \ll 2\Delta$,
 356 placing this material in the clean limit; as a result, most
 357 of the weight in the condensate will come from this band.
 358 In the broad Drude band, $1/\tau_{D2} > 2\Delta$, placing this band
 359 in the dirty limit; consequently, only a small fraction of
 360 the weight in this band will collapse into the conden-
 361 sate. This is another example of a multiband iron-based
 362 superconductor that is simultaneously in both the clean
 363 and dirty limits [61]. One of the interesting properties
 364 of this material is its relatively low resistivity just above
 365 T_c , $\rho_{ab} \simeq 20 \mu\Omega \text{ cm}$, or $\sigma_{dc} \simeq 5 \times 10^4 \Omega^{-1} \text{ cm}^{-1}$ [Fig 1].
 366 These values place this material just below the univer-

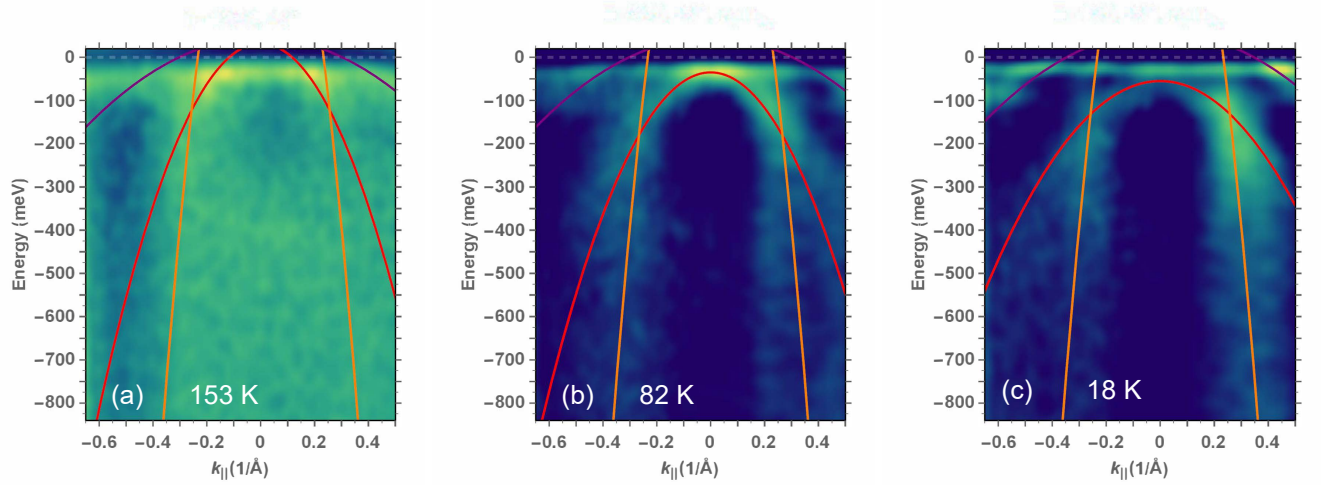


Figure 6. The temperature dependence of the second-derivative of the hole-like bands of $\text{Sr}_{0.67}\text{Na}_{0.33}\text{Fe}_2\text{As}_2$ around the Γ point along the $\Gamma \rightarrow \text{M}$ cut at: (a) above T_N at 153 K, (b) for $T_r < T < T_N$ at 82 K, and (c) below T_r at 18 K. At high temperature three hole-like bands may be resolved that cross ϵ_F . Below T_N two of these bands shift to below the Fermi level; this trend continues below T_r as the bands shift further below ϵ_F . The lines are drawn as a guide to the eye.

367 sal scaling line $\rho_s(T \ll T_c) \propto \sigma_{dc}(T \gtrsim T_c) T_c$ [62–64], in 394
 368 close proximity to other doped “122” superconductors,
 369 as well as many cuprate materials [65].

B. Low-energy peak

370
 371 The dramatic collapse of the scattering rate below T_r
 372 of the narrow Drude allows a new low-energy peak at
 373 $\omega_0 \simeq 170 \text{ cm}^{-1}$, with width $\gamma_0 \simeq 110 \text{ cm}^{-1}$ and oscillator
 374 strength of $\Omega_0 \simeq 2230 \text{ cm}^{-1}$, to be observed [Figs. 2(a),
 375 3(c), and supplementary Fig. S2]. This is close to where
 376 a peak was observed in $(\text{CaFe}_{1-x}\text{Pt}_x\text{As})_{10}\text{Pt}_3\text{As}_8$ for $x =$
 377 0.1 at $\simeq 120 \text{ cm}^{-1}$ [66]; that feature was attributed to a
 378 localization process due to impurity scattering described
 379 by a classical generalization of the Drude model [67],

$$\tilde{\sigma}(\omega) = \left(\frac{2\pi}{Z_0} \right) \frac{\omega_p^2 \tau}{(1 - i\omega\tau)} \left[1 + \frac{c}{(1 - i\omega\tau)} \right], \quad (2)$$

380 where c is the persistence of velocity that is retained 414
 381 for a single collision. The scattering rate for the narrow 415
 382 Drude is far too small to yield a peak at the 416
 383 experimentally-observed position, while the broad Drude 417
 384 predicts a localization peak at $\simeq 120 \text{ cm}^{-1}$, well below 418
 385 the experimentally-observed value of $\omega_0 \simeq 170 \text{ cm}^{-1}$ [68]. 419
 386 Thus, it is likely that the low-energy peak originates from 420
 387 a further reconstruction of the Fermi surface in the C_4 421
 388 phase rather than any sort of localization process. In- 422
 389 deed, a remarkably similar peak has also been observed 423
 390 to emerge at $\simeq 150 \text{ cm}^{-1}$ in the optical conductivity 424
 391 of underdoped $\text{Ba}_{1-x}\text{K}_x\text{Fe}_2\text{As}_2$ at low temperature [69]; 425
 392 this feature may also be related to the magnetic C_4 426
 393 phase observed in that compound.

C. ARPES

395 A simple density functional theory calculation of
 396 SrFe_2As_2 in the paramagnetic high-temperature tetrago-
 397 nal phase reveals a familiar band structure consisting of
 398 three hole-like pockets at the center of the Brillouin zone
 399 (Γ), and two electron-like pockets at the corners (M); the
 400 orbital character is primarily Fe d_{xz}/d_{yz} in nature (shown
 401 in supplementary Fig. S4, details of the calculation are
 402 discussed in the Supplementary Material.) The Fermi
 403 surface of $\text{Sr}_{0.67}\text{Na}_{0.33}\text{Fe}_2\text{As}_2$, with the spectral weight
 404 integrated within a $\pm 10 \text{ meV}$ energy window with re-
 405 spect to the Fermi level, is shown below T_r in the C_4
 406 magnetic phase at 23 K, in Fig. 5(a). Two momentum
 407 cuts have been made along the $\Gamma \rightarrow \text{M}$ path; the first
 408 examines the temperature dependence of the anisotropic
 409 electron-like bands around an M point, Fig. 5(b), and the
 410 second details the behavior of the isotropic hole-like pock-
 411 ets around the Γ point, shown in Fig. 5(c). This Fermi
 412 surface is qualitatively similar to what was observed in
 413 $\text{Ba}_{1-x}\text{K}_x\text{Fe}_2\text{As}_2$ [70, 71]

414 At high temperature, the cut along the $\Gamma \rightarrow \text{M}$ direc-
 415 tion at the M point there appears to be a hole-like band
 416 as well as a possible electron-like band at 135 K, shown
 417 in the upper panel of Fig. 5(b). In the simple picture for
 418 the Fermi surface of SrFe_2As_2 (supplementary Fig. S4)
 419 this result can be reproduced by lowering the Fermi level
 420 ϵ_F by about 0.2 eV, which is consistent with the removal
 421 of electrons due to sodium substitution (hole doping). As
 422 the temperature is lowered below T_N and enters the mag-
 423 netic C_2 phase, the hole-like band may split, while the
 424 electron-like band appears to shift below ϵ_F . Below T_r in
 425 the C_4 magnetic phase, a single hole-like band is recov-
 426 ered, while the electron-like band now appears to be split
 427 into two bands, with a separation of $\simeq 20 \text{ meV}$, which is

comparable to the position of the low-energy peak (this behavior is explored further in supplementary Fig. S5).

The initial investigation into the temperature dependence of the energy bands around the Γ point in Fig. 5(c) revealed two large hole pockets at the Fermi level, but relatively little temperature dependence. This prompted a more detailed investigation of the hole-like bands along the $\Gamma \rightarrow M$ path, shown in Fig. 6 (further detail is provided in supplementary Figs. S6 and S7). Above T_N the bands are rather broad, but at least three bands may be resolved, all of which cross the Fermi level, resulting in several large hole-like Fermi surfaces, shown in the second-derivative curves in Fig. 6(a). Below T_N the bands sharpen considerably in the C_2 phase, and one of the bands is observed to shift to $\simeq 40$ meV below the Fermi level, shown in Fig. 6(b), leading to the removal of a hole-like Fermi surface; this is consistent with the Fermi surface reconstruction below T_N observed in the parent compounds [58, 72]. This trend continues in the magnetic C_4 phase, with the band shifting to $\simeq 60$ meV below the Fermi level, Fig. 6(c).

D. Discussion

Both the electron and hole pockets appear to undergo significant changes in response to the Fermi surface reconstruction in the magnetic C_2 and C_4 phases that exhibit SDW and CSDW order, respectively. In the case of the hole pockets, the fact that one of the bands shifts below ϵ_F below T_N in the magnetic C_2 phase, shifting further below T_r in the magnetic C_4 phase, signals the decrease in the size of the Fermi surface associated with the hole pockets. It is possible that this may be related to the dramatic decrease in the spectral weight of the broad Drude component as described by the plasma frequency in Fig. 4(a); from $\omega_{p,D2}^2 \propto n/m^*$ we infer a significant decrease in the carriers associated with the hole pockets at low temperature ($\simeq 90\%$ reduction of the room temperature value).

The evolution of the electron-like bands is more complicated, as the bands at the M point have both electron- and hole-like character. The initial splitting of the hole-like band below T_N is consistent with the lifting of the degeneracy between the d_{xz} and d_{yz} orbitals; however, the fact that one of the hole-like bands lies completely below the Fermi level suggests no significant changes to the size of the Fermi surfaces. Below T_r the orbital degeneracy is restored, but the presence of CSDW order leads to the formation of a supercell; the electron-like bands are split as a result of zone-folding, which may lead to an increase in the size of the Fermi surface. This is consistent with the slight increase in the plasma frequency of the narrow Drude component at low temperature, shown in Fig. 4(a). Furthermore, the splitting between the two electron-like bands of $\simeq 20$ meV, is very close to the position of the low-energy peak. This suggests that, similar to the mid-infrared peak, the low-energy peak emerges in response to the Fermi surface reconstruction driven

by the C_4 magnetic phase and the CSDW order at low temperature [43].

IV. SUMMARY

The ARPES and complex optical properties of freshly-cleaved surfaces of the iron-based superconductor $\text{Sr}_{0.67}\text{Na}_{0.33}\text{Fe}_2\text{As}_2$ have been determined for light polarized in the iron-arsenic (a - b) planes at a variety of temperatures for the room temperature tetragonal paramagnetic phase, the orthorhombic C_2 SDW magnetic phase, the tetragonal C_4 double- \mathbf{Q} SDW (CSDW) phase, as well as below T_c in the superconducting state. The free-carrier response is described by two Drude components, one broad and strong, the other narrow and weak. The strength of the narrow component shows little temperature dependence, increasing slightly in strength at low temperature, while narrowing dramatically. The broad Drude component decreases dramatically in strength and narrows below T_N at the same time a peak emerges in the mid-infrared; the decrease in the spectral weight associated with the free carriers is transferred into the emergent peak. Below T_r , this trend continues, with the emergence of a new low-energy peak at $\simeq 20$ meV. The appearance of a new infrared-active mode in the Fe-As planes below T_r is attributed to zone-folding due to the formation of a supercell in response to the CSDW; this suggests that the low-energy peak originates from a further Fermi surface reconstruction in the C_4 phase. Below T_c the low-frequency conductivity decreases dramatically, signalling the formation of a superconducting energy gap. ARPES reveals large hole-like Fermi surfaces at the Γ point, one of which is apparently removed below the structural and magnetic transitions, suggesting that they may be related to the behavior of the broad Drude component. The electron- and hole-like bands at the corners of the Brillouin zone shift and split below T_N and T_r , but the Fermi surfaces do not appear to undergo any significant change in size, suggesting they may be related to the narrow Drude component; the apparent splitting of the electron-like bands in the C_4 phase would appear to explain the emergence of the low-energy peak at $\simeq 20$ meV in the optical conductivity. While the C_2 and C_4 magnetic transitions, with resulting SDW and CSDW order, respectively, lead to a significant reconstruction of the Fermi surface that has profound implications for the transport originating from the electron- and hole-like pockets, they appear to have relatively little impact on the superconductivity in this material.

ACKNOWLEDGMENTS

Work at Chinese Academy of Science was supported by NSFC (Project Nos. 11774400, 11888101, and 11974412) and MOST (Project Nos. 2015CB921102, 2016YFA0300300, and 2017YFA0302903). Work at HP-

536 STAR was supported by NSAF, Grant No. U1530402. 538 by the Office of Science, U.S. Department of Energy un-
537 Work at Brookhaven National Laboratory was supported 539 der Contract No. DE-SC0012704.

- 540 [1] David C. Johnston, “The puzzle of high temperature 597
541 superconductivity in layered iron pnictides and chalcogenides,” *Adv. Phys.* **59**, 803–1061 (2010). 598
- 542 [2] Johnpierre Paglione and Richard L. Greene, “High- 599
543 temperature superconductivity in iron-based materials,” 600
544 *Nat. Phys.* **6**, 645–658 (2010). 601
- 545 [3] Paul C. Canfield and Sergey L. Bud’ko, “FeAs-Based Su- 602
546 perconductivity: A Case Study of the Effects of Transi- 603
547 tion Metal Doping on BaFe_2As_2 ,” *Ann. Rev. Cond. Mat.* 604
548 *Phys.* **1**, 27–50 (2010). 605
- 549 [4] Qimiao Si, Rong Yu, and Elihu Abrahams, “High- 606
550 temperature superconductivity in iron pnictides and 607
551 chalcogenides,” *Nat. Rev. Mater.* **1**, 16017 (2016). 608
- 552 [5] M. P. M. Dean, M. G. Kim, A. Kreyssig, J. W. 609
553 Kim, X. Liu, P. J. Ryan, A. Thaler, S. L. Bud’ko, 610
554 W. Strassheim, P. C. Canfield, J. P. Hill, and A. I. 611
555 Goldman, “Magnetically polarized Ir dopant atoms in 612
556 superconducting $\text{Ba}(\text{Fe}_{1-x}\text{Ir}_x)_2\text{As}_2$,” *Phys. Rev. B* **85**, 613
557 140514(R) (2012). 614
- 558 [6] Pengcheng Dai, “Antiferromagnetic order and spin 615
559 dynamics in iron-based superconductors,” *Rev. Mod. Phys.* 616
560 **87**, 855–896 (2015). 617
- 561 [7] M. Moroni, P. Carretta, G. Allodi, R. De Renzi, M. N. 618
562 Gastiasoro, B. M. Andersen, P. Materne, H.-H. Klaus, 619
563 Y. Kobayashi, M. Sato, and S. Sanna, “Fast recovery 620
564 of the stripe magnetic order by Mn/Fe substitution in 621
565 F-doped LaFeAsO superconductors,” *Phys. Rev. B* **95**, 622
566 180501(R) (2017). 623
- 567 [8] A. Kreyssig, J. M. Wilde, A. E. Böhmer, W. Tian, W. R. 624
568 Meier, Bing Li, B. G. Ueland, Mingyu Xu, S. L. Bud’ko, 625
569 P. C. Canfield, R. J. McQueeney, and A. I. Gold- 626
570 man, “Antiferromagnetic order in $\text{CaK}(\text{Fe}_{1-x}\text{Ni}_x)_4\text{As}_4$ 627
571 and its interplay with superconductivity,” *Phys. Rev. B* 628
572 **97**, 224521 (2018). 629
- 573 [9] William R. Meier, Qing-Ping Ding, Andreas Kreyssig, 630
574 Sergey L. Bud’ko, Aashish Sapkota, Karunakar Kotha- 631
575 palli, Vladislav Borisov, Roser Valentí, Cristian D. 632
576 Batista, Peter P. Orth, Rafael M. Fernandes, Alan I. 633
577 Goldman, Yuji Furukawa, Anna E. Böhmer, and Paul C. 634
578 Canfield, “Hedgehog spin-vortex crystal stabilized in a 635
579 hole-doped iron-based superconductor,” *npj Quantum* 636
580 *Materials* **3**, 5 (2018). 637
- 581 [10] Marianne Rotter, Marcus Tegel, and Dirk Johrendt, 638
582 “Superconductivity at 38 K in the Iron Arsenide 639
583 $(\text{Ba}_{1-x}\text{K}_x)\text{Fe}_2\text{As}_2$,” *Phys. Rev. Lett.* **101**, 107006 (2008). 640
- 584 [11] Athena S. Sefat, Rongying Jin, Michael A. McGuire, 641
585 Brian C. Sales, David J. Singh, and David Mandrus, 642
586 “Superconductivity at 22 K in Co-Doped BaFe_2As_2 Crys- 643
587 tals,” *Phys. Rev. Lett.* **101**, 117004 (2008). 644
- 588 [12] N. Ni, M. E. Tillman, J.-Q. Yan, A. Kracher, S. T. Han- 645
589 nahs, S. L. Bud’ko, and P. C. Canfield, “Effects of Co 646
590 substitution on thermodynamic and transport properties 647
591 and anisotropic H_{c2} in $\text{Ba}(\text{Fe}_{1-x}\text{Co}_x)_2\text{As}_2$ single crys- 648
592 tals,” *Phys. Rev. B* **78**, 214515 (2008). 649
- 593 [13] Kalyan Sasmal, Bing Lv, Bernd Lorenz, Arnold M. Gu- 650
594 loy, Feng Chen, Yu-Yi Xue, and Ching-Wu Chu, “Super- 651
595 conducting Fe-Based Compounds $(\text{A}_{1-x}\text{Sr}_x)\text{Fe}_2\text{As}_2$ with 652
596 $\text{A} = \text{K}$ and Cs with Transition Temperatures up to 37 K,” 653
Phys. Rev. Lett. **101**, 107007 (2008).
- [14] Gen-Fu Chen, Zheng Li, Gang Li, Wan-Zheng Hu, Jing 654
Dong, Xiao-Dong Zhang Jun Zhou, Ping Zheng, Nan-Lin 655
Wang, and Jian-Lin Luo, “Superconductivity in Hole- 656
Doped $(\text{Sr}_{1-x}\text{K}_x)\text{Fe}_2\text{As}_2$,” *Chin. Phys. Lett.* **25**, 3403 657
(2008).
- [15] Jiun-Haw Chu, James G. Analytis, Chris Kucharczyk, 658
and Ian R. Fisher, “Determination of the 659
phase diagram of the electron-doped superconductor 660
 $\text{Ba}(\text{Fe}_{1-x}\text{Co}_x)_2\text{As}_2$,” *Phys. Rev. B* **79**, 014506 (2009). 661
- [16] T. Goko, A. A. Aczel, E. Baggio-Saitovitch, S. L. Bud’ko, 662
P. C. Canfield, J. P. Carlo, G. F. Chen, Pengcheng Dai, 663
A. C. Hamann, W. Z. Hu, H. Kageyama, G. M. Luke, 664
J. L. Luo, B. Nachumi, N. Ni, D. Reznik, D. R. Sanchez- 665
Candela, A. T. Savici, K. J. Sikes, N. L. Wang, C. R. 666
Wiebe, T. J. Williams, T. Yamamoto, W. Yu, and 667
Y. J. Uemura, “Superconducting state coexisting with a 668
phase-separated static magnetic order in $(\text{Ba},\text{K})\text{Fe}_2\text{As}_2$, 669
 $(\text{Sr},\text{Na})\text{Fe}_2\text{As}_2$, and CaFe_2As_2 ,” *Phys. Rev. B* **80**, 024508 670
(2009). 671
- [17] S. R. Saha, N. P. Butch, K. Kirshenbaum, and John- 672
pierre Paglione, “Evolution of bulk superconductivity in 673
 SrFe_2As_2 with Ni substitution,” *Phys. Rev. B* **79**, 224519 674
(2009). 675
- [18] Shuai Jiang, Hui Xing, Guofang Xuan, Cao Wang, 676
Zhi Ren, Chunmu Feng, Jianhui Dai, Zhu’an Xu, 677
and Guanghan Cao, “Superconductivity up to 30 K 678
in the vicinity of the quantum critical point in 679
 $\text{BaFe}_2(\text{As}_{1-x}\text{P}_x)_2$,” *J. Phys.: Condens. Matter* **21**, 382203 680
(2009). 681
- [19] H. L. Shi, H. X. Yang, H. F. Tian, J. B. Lu, Z. W. 682
Wang, Y. B. Qin, Y. J. Song, and J. Q. Li, “Structural 683
properties and superconductivity of $\text{SrFe}_2\text{As}_{2-x}\text{P}_x$ and 684
 $(0.0 \leq x \leq 1.0)$ and $\text{CaFe}_2\text{As}_{2-y}\text{P}_y$ $(0.0 \leq y \leq 0.3)$,” *J.* 685
Phys.: Condens. Matter **22**, 125702 (2010). 686
- [20] Raquel Cortes-Gil and Simon J. Clarke, “Structure, Mag- 687
netism, and Superconductivity of the Layered Iron Ar- 688
senides $\text{Sr}_{1-x}\text{Na}_x\text{Fe}_2\text{As}_2$,” *Chem. Mater.* **23**, 1009–1016 689
(2011). 690
- [21] Fumihiko Ishikawa, Naoya Eguchi, Michihiro Kodama, 691
Koji Fujimaki, Mari Einaga, Ayako Ohmura, Atsuko 692
Nakayama, Akihiro Mitsuda, and Yuh Yamada, “Zero- 693
resistance superconducting phase in BaFe_2As_2 under 694
high pressure,” *Phys. Rev. B* **79**, 172506 (2009). 695
- [22] Patricia L. Alireza, Y. T. Chris Ko, Jack Gillett, 696
Chiara M. Petrone, Jacqui M. Cole, Suchitra E. Sebas- 697
tian, and Gilbert G. Lonzarich, “Superconductivity up 698
to 29 K in SrFe_2As_2 and BaFe_2As_2 at high pressures,” *J.* 699
Phys: Cond. Matter **21**, 012208 (2009). 700
- [23] E. Colombier, S. L. Bud’ko, N. Ni, and P. C. Can- 701
field, “Complete pressure-dependent phase diagrams for 702
 SrFe_2As_2 and BaFe_2As_2 ,” *Phys. Rev. B* **79**, 224518 703
(2009). 704
- [24] K. Kitagawa, N. Katayama, H. Gotou, T. Yagi, K. Oh- 705
gushi, T. Matsumoto, Y. Uwatoko, and M. Takigawa, 706
“Spontaneous Formation of a Superconducting and Anti-

- ferromagnetic Hybrid State in SrFe_2As_2 under High Pressure,” *Phys. Rev. Lett.* **103**, 257002 (2009).
- [25] Marcus Tegel, Marianne Rotter, Veronika Weiß, Falko M Schappacher, Rainer Pöttgen, and Dirk Johrendt, “Structural and magnetic phase transitions in the ternary iron arsenides SrFe_2As_2 and EuFe_2As_2 ,” *J. Phys.: Condens. Matter* **20**, 452201 (2008).
- [26] J.-Q. Yan, A. Kreyssig, S. Nandi, N. Ni, S. L. Bud’ko, A. Kracher, R. J. McQueeney, R. W. McCallum, T. A. Lograsso, A. I. Goldman, and P. C. Canfield, “Structural transition and anisotropic properties of single-crystalline SrFe_2As_2 ,” *Phys. Rev. B* **78**, 024516 (2008).
- [27] Jun Zhao, W. Ratcliff, J. W. Lynn, G. F. Chen, J. L. Luo, N. L. Wang, Jiangping Hu, and Pengcheng Dai, “Spin and lattice structures of single-crystalline SrFe_2As_2 ,” *Phys. Rev. B* **78**, 140504(R) (2008).
- [28] W. Z. Hu, J. Dong, G. Li, Z. Li, P. Zheng, G. F. Chen, J. L. Luo, and N. L. Wang, “Origin of the Spin Density Wave Instability in AFe_2As_2 ($A=\text{Ba}, \text{Sr}$) as Revealed by Optical Spectroscopy,” *Phys. Rev. Lett.* **101**, 257005 (2008).
- [29] J. N. Hancock, S. I. Mirzaei, J. Gillett, S. E. Sebastian, J. Teyssier, R. Vienneis, E. Giannini, and D. van der Marel, “Strong coupling to magnetic fluctuations in the charge dynamics of iron-based superconductors,” *Phys. Rev. B* **82**, 014523 (2010).
- [30] E. C. Blomberg, M. A. Tanatar, A. Kreyssig, N. Ni, A. Thaler, Rongwei Hu, S. L. Bud’ko, P. C. Canfield, A. I. Goldman, and R. Prozorov, “In-plane anisotropy of electrical resistivity in strain-detwinned SrFe_2As_2 ,” *Phys. Rev. B* **83**, 134505 (2011).
- [31] M. A. Tanatar, A. Kreyssig, S. Nandi, N. Ni, S. L. Bud’ko, P. C. Canfield, A. I. Goldman, and R. Prozorov, “Direct imaging of the structural domains in the iron pnictides AFe_2As_2 ($A = \text{Ca}, \text{Sr}, \text{Ba}$),” *Phys. Rev. B* **79**, 180508(R) (2009).
- [32] I. R. Fisher, L. Degiorgi, and Z. X. Shen, “In-plane electronic anisotropy of underdoped ‘122’ Fe-arsenide superconductors revealed by measurements of detwinned single crystals,” *Rep. Prog. Phys.* **74**, 124506 (2011).
- [33] A. I. Goldman, D. N. Argyriou, B. Ouladdiaf, T. Chatterji, A. Kreyssig, S. Nandi, N. Ni, S. L. Bud’ko, P. C. Canfield, and R. J. McQueeney, “Lattice and magnetic instabilities in CaFe_2As_2 : A single-crystal neutron diffraction study,” *Phys. Rev. B* **78**, 100506(R) (2008).
- [34] M. Kofu, Y. Qiu, Wei Bao, S.-H. Lee, S. Chang, T. Wu, G. Wu, and X. H. Chen, “Neutron scattering investigation of the magnetic order in single crystalline BaFe_2As_2 ,” *New J. Phys.* **11**, 055001 (2009).
- [35] M. G. Kim, A. Kreyssig, A. Thaler, D. K. Pratt, W. Tian, J. L. Zarestky, M. A. Green, S. L. Bud’ko, P. C. Canfield, R. J. McQueeney, and A. I. Goldman, “Antiferromagnetic ordering in the absence of structural distortion in $\text{Ba}(\text{Fe}_{1-x}\text{Mn}_x)_2\text{As}_2$,” *Phys. Rev. B* **82**, 220503(R) (2010).
- [36] E. Hassinger, G. Gredat, F. Valade, S. René de Cotret, A. Juneau-Fecteau, J.-Ph. Reid, H. Kim, M. A. Tanatar, R. Prozorov, B. Shen, H.-H. Wen, N. Doiron-Leyraud, and Louis Taillefer, “Pressure-induced Fermi-surface reconstruction in the iron-arsenide superconductor $\text{Ba}_{1-x}\text{K}_x\text{Fe}_2\text{As}_2$: Evidence of a phase transition inside the antiferromagnetic phase,” *Phys. Rev. B* **86**, 140502(R) (2012).
- [37] A. E. Böhmer, F. Hardy, L. Wang, T. Wolf, P. Schweiss, and C. Meingast, “Superconductivity-induced re-entrance of the orthorhombic distortion in $\text{Ba}_{1-x}\text{K}_x\text{Fe}_2\text{As}_2$,” *Nat. Commun.* **6**, 7911 (2015).
- [38] L. Wang, F. Hardy, A. E. Böhmer, T. Wolf, P. Schweiss, and C. Meingast, “Complex phase diagram of $\text{Ba}_{1-x}\text{Na}_x\text{Fe}_2\text{As}_2$: A multitude of phases striving for the electronic entropy,” *Phys. Rev. B* **93**, 014514 (2016).
- [39] K. M. Taddei, J. M. Allred, D. E. Bugaris, S. Lapidus, M. J. Krogstad, R. Stadel, H. Claus, D. Y. Chung, M. G. Kanatzidis, S. Rosenkranz, R. Osborn, and O. Chmaissem, “Detailed magnetic and structural analysis mapping a robust magnetic C_4 dome in $\text{Sr}_{1-x}\text{Na}_x\text{Fe}_2\text{As}_2$,” *Phys. Rev. B* **93**, 134510 (2016).
- [40] Liran Wang, Mingquan He, Daniel D. Scherer, Frédéric Hardy, Peter Schweiss, Thomas Wolf, Michael Merz, Brian M. Andersen, and Christoph Meingast, “Competing Electronic Phases near the Onset of Superconductivity in Hole-doped SrFe_2As_2 ,” *J. Phys. Soc. Jpn.* **88**, 104710 (2019).
- [41] E. Hassinger, G. Gredat, F. Valade, S. René de Cotret, O. Cyr-Choinière, A. Juneau-Fecteau, J.-Ph. Reid, H. Kim, M. A. Tanatar, R. Prozorov, B. Shen, H.-H. Wen, N. Doiron-Leyraud, and Louis Taillefer, “Expansion of the tetragonal magnetic phase with pressure in the iron arsenide superconductor $\text{Ba}_{1-x}\text{K}_x\text{Fe}_2\text{As}_2$,” *Phys. Rev. B* **93**, 144401 (2016).
- [42] K. M. Taddei, J. M. Allred, D. E. Bugaris, S. H. Lapidus, M. J. Krogstad, H. Claus, D. Y. Chung, M. G. Kanatzidis, R. Osborn, S. Rosenkranz, and O. Chmaissem, “Observation of the magnetic C_4 phase in $\text{Ca}_{1-x}\text{Na}_x\text{Fe}_2\text{As}_2$ and its universality in the hole-doped 122 superconductors,” *Phys. Rev. B* **95**, 064508 (2017).
- [43] M. Yi, A. Frano, D. H. Lu, Y. He, Meng Wang, B. A. Frandsen, A. F. Kemper, R. Yu, Q. Si, L. Wang, M. He, F. Hardy, P. Schweiss, P. Adelman, T. Wolf, M. Hashimoto, S.-K. Mo, Z. Hussain, M. Le Tacon, A. E. Böhmer, D.-H. Lee, Z.-X. Shen, C. Meingast, and R. J. Birgeneau, “Spectral Evidence for Emergent Order in $\text{Ba}_{1-x}\text{Na}_x\text{Fe}_2\text{As}_2$,” *Phys. Rev. Lett.* **121**, 127001 (2018).
- [44] S. Avci, O. Chmaissem, J. M. Allred, S. Rosenkranz, I. Eremin, A. V. Chubukov, D. E. Bugaris, D. Y. Chung, M. G. Kanatzidis, J.-P. Castellan, J. A. Schlueter, H. Claus, D. D. Khalyavin, P. Manuel, A. Daoud-Aladine, and R. Osborn, “Magnetically driven suppression of nematic order in an iron-based superconductor,” *Nat. Commun.* **5**, 3845 (2014).
- [45] J. M. Allred, K. M. Taddei, D. E. Bugaris, M. J. Krogstad, S. H. Lapidus, D. Y. Chung, H. Claus, M. G. Kanatzidis, D. E. Brown, J. Kang, R. M. Fernandes, I. Eremin, S. Rosenkranz, O. Chmaissem, and R. Osborn, “Double-Q spin-density wave in iron arsenide superconductors,” *Nat. Phys.* **12**, 493 (2016).
- [46] F. Waßer, A. Schneidewind, Y. Sidis, S. Wurmehl, S. Aswartham, B. Büchner, and M. Braden, “Spin reorientation in $\text{Ba}_{0.65}\text{Na}_{0.35}\text{Fe}_2\text{As}_2$ studied by single-crystal neutron diffraction,” *Phys. Rev. B* **91**, 060505(R) (2015).
- [47] B. P. P. Mallett, Yu. G. Pashkevich, A. Gusev, Th. Wolf, and C. Bernhard, “Muon spin rotation study of the magnetic structure in the tetragonal antiferromagnetic state of weakly underdoped $\text{Ba}_{1-x}\text{K}_x\text{Fe}_2\text{As}_2$,” *EPL (Europhysics Letters)* **111**, 57001 (2015).
- [48] Mareike Hoyer, Rafael M. Fernandes, Alex Levchenko, and Jörg Schmalian, “Disorder-promoted C_4 -symmetric

- magnetic order in iron-based superconductors,” Phys. Rev. B **93**, 144414 (2016).
- [49] Jianqing Guo, Li Yue, Kazuki Iida, Kazuya Kamazawa, Lei Chen, Tingting Han, Yan Zhang, and Yuan Li, “Preferred magnetic excitations in the iron-based $\text{Sr}_{1-x}\text{Na}_x\text{Fe}_2\text{As}_2$ superconductor,” Phys. Rev. Lett. **122**, 017001 (2019).
- [50] Christopher C. Homes, M. Reedyk, D. A. Crandles, and T. Timusk, “Technique for measuring the reflectance of irregular, submillimeter-sized samples,” Appl. Opt. **32**, 2976–2983 (1993).
- [51] See Supplemental Material at [URL will be inserted by publisher] for details of the experimental reflectivity and Kramers-Kronig analysis, which includes Refs. 73–77.
- [52] Y. M. Dai, Ana Akrap, S. L. Bud’ko, P. C. Canfield, and C. C. Homes, “Optical properties of AFe_2As_2 ($A = \text{Ca}$, Sr , and Ba) single crystals,” Phys. Rev. B **94**, 195142 (2016).
- [53] C. C. Homes, Y. M. Dai, Ana Akrap, S. L. Bud’ko, and P. C. Canfield, “Vibrational anomalies in AFe_2As_2 ($A = \text{Ca}$, Sr , and Ba) single crystals,” Phys. Rev. B **98**, 035103 (2018).
- [54] B. P. P. Mallett, P. Marsik, M. Yazdi-Rizi, Th. Wolf, A. E. Böhmer, F. Hardy, C. Meingast, D. Munzar, and C. Bernhard, “Infrared Study of the Spin Reorientation Transition and Its Reversal in the Superconducting State in Underdoped $\text{Ba}_{1-x}\text{K}_x\text{Fe}_2\text{As}_2$,” Phys. Rev. Lett. **115**, 027003 (2015).
- [55] D. J. Singh, “Electronic structure and doping in BaFe_2As_2 and LiFeAs : Density functional calculations,” Phys. Rev. B **78**, 094511 (2008).
- [56] J. Fink, S. Thirupathiah, R. Ovsyannikov, H. A. Dürr, R. Follath, Y. Huang, S. de Jong, M. S. Golden, Yu-Zhong Zhang, H. O. Jeschke, R. Valentí, C. Felser, S. Dastjani Farahani, M. Rotter, and D. Johrendt, “Electronic structure studies of BaFe_2As_2 by angle-resolved photoemission spectroscopy,” Phys. Rev. B **79**, 155118 (2009).
- [57] D. Wu, N. Barišić, P. Kallina, A. Faridian, B. Gorshunov, N. Drichko, L. J. Li, G. Lin, G. H. Cao, Z. A. Xu, N. L. Wang, and M. Dressel, “Optical investigations of the normal and superconducting states reveal two electronic subsystems in iron pnictides,” Phys. Rev. B **81**, 100512(R) (2010).
- [58] Z. P. Yin, K. Haule, and G. Kotliar, “Magnetism and charge dynamics in iron pnictides,” Nat. Phys. **7**, 294–297 (2011).
- [59] Richard A. Ferrell and Rolfe E. Glover, “Conductivity of Superconducting Films: A Sum Rule,” Phys. Rev. **109**, 1398–1399 (1958).
- [60] M. Tinkham and R. A. Ferrell, “Determination of the Superconducting Skin Depth from the Energy Gap and Sum Rule,” Phys. Rev. Lett. **2**, 331–333 (1959).
- [61] C. C. Homes, Y. M. Dai, J. S. Wen, Z. J. Xu, and G. D. Gu, “ $\text{FeTe}_{0.55}\text{Se}_{0.45}$: A multiband superconductor in the clean and dirty limit,” Phys. Rev. B **91**, 144503 (2015).
- [62] C. C. Homes, S. V. Dordevic, M. Strongin, D. A. Bonn, Ruixing Liang, W. N. Hardy, Seiki Komiya, Yoichi Ando, G. Yu, N. Kaneko, X. Zhao, M. Greven, D. N. Basov, and T. Timusk, “Universal scaling relation in high-temperature superconductors,” Nature (London) **430**, 539 (2004).
- [63] C. C. Homes, S. V. Dordevic, D. A. Bonn, Ruixing Liang, W. N. Hardy, and T. Timusk, “Coherence, incoherence, and scaling along the c axis of $\text{YBa}_2\text{Cu}_3\text{O}_{6+x}$,” Phys. Rev. B **71**, 184515 (2005).
- [64] C. C. Homes, S. V. Dordevic, T. Valla, and M. Strongin, “Scaling of the superfluid density in high-temperature superconductors,” Phys. Rev. B **72**, 134517 (2005).
- [65] J. J. Tu, J. Li, W. Liu, A. Punnoose, Y. Gong, Y. H. Ren, L. J. Li, G. H. Cao, Z. A. Xu, and C. C. Homes, “Optical properties of the iron arsenic superconductor $\text{BaFe}_{1.85}\text{Co}_{0.15}\text{As}_2$,” Phys. Rev. B **82**, 174509 (2010).
- [66] Run Yang, Yaomin Dai, Jia Yu, Qiangtao Sui, Yongqing Cai, Zhian Ren, Jungseek Hwang, Hong Xiao, Xingjiang Zhou, Xianggang Qiu, and Christopher C. Homes, “Unravelling the mechanism of the semiconducting-like behavior and its relation to superconductivity in $(\text{CaFe}_{1-x}\text{Pt}_x\text{As})_{10}\text{Pt}_3\text{As}_8$,” Phys. Rev. B **99**, 144520 (2019).
- [67] N. V. Smith, “Classical generalization of the Drude formula for the optical conductivity,” Phys. Rev. B **64**, 155106 (2001).
- [68] Replacing the broad Drude term with the expression in Eq. (2) and fitting to the real and imaginary parts of the optical conductivity using a non-linear least-squares technique yields $\omega_p \simeq 5350 \text{ cm}^{-1}$, $1/\tau \simeq 146 \text{ cm}^{-1}$, and $c = -0.7$. The plasma frequency is larger because it now describes both the localized as well as free carriers; $\omega_p^2 \simeq \omega_{p,D2}^2 + \Omega_0^2$.
- [69] Y. M. Dai, B. Xu, B. Shen, H. H. Wen, J. P. Hu, X. G. Qiu, and R. P. S. M. Lobo, “Pseudogap in underdoped $\text{Ba}_{1-x}\text{K}_x\text{Fe}_2\text{As}_2$ as seen via optical conductivity,” Phys. Rev. B **86**, 100501(R) (2012).
- [70] V. B. Zabolotnyy, D. S. Inosov, D. V. Evtushinsky, A. Koitzsch, A. A. Kordyuk, G. L. Sun, J. T. Park, D. Haug, V. Hinkov, A. V. Boris, C. T. Lin, M. Knupfer, A. N. Yaresko, B. Büchner, A. Varykhalov, R. Follath, and S. V. Borisenko, “ (π, π) electronic order in iron arsenide superconductors,” Nature **457**, 569–572 (2009).
- [71] Gerald Derondeau, Federico Bisti, Masaki Kobayashi, Jürgen Braun, Hubert Ebert, Victor A. Rogalev, Ming Shi, Thorsten Schmitt, Junzhang Ma, Hong Ding, Vladimir N. Strocov, and Ján Minár, “Fermi surface and effective masses in photoemission response of the $(\text{Ba}_{1-x}\text{K}_x)\text{Fe}_2\text{As}_2$ superconductor,” Sci. Rep. **7**, 8787 (2017).
- [72] M. Yi, D. H. Lu, J. G. Analytis, J.-H. Chu, S.-K. Mo, R.-H. He, M. Hashimoto, R. G. Moore, I. I. Mazin, D. J. Singh, Z. Hussain, I. R. Fisher, and Z.-X. Shen, “Unconventional electronic reconstruction in undoped $(\text{Ba},\text{Sr})\text{Fe}_2\text{As}_2$ across the spin density wave transition,” Phys. Rev. B **80**, 174510 (2009).
- [73] F. Wooten, *Optical Properties of Solids* (Academic Press, New York, 1972) pp. 244–250.
- [74] M. Dressel and G. Grüner, *Electrodynamics of Solids* (Cambridge University Press, Cambridge, 2001).
- [75] D. J. Singh, *Planewaves, Pseudopotentials and the LAPW method* (Kluwer Academic, Boston, 1994).
- [76] David Singh, “Ground-state properties of lanthanum: Treatment of extended-core states,” Phys. Rev. B **43**, 6388–6392 (1991).
- [77] P. Blaha, K. Schwarz, G. K. H. Madsen, D. Kvasnicka and J. Luitz, WIEN2k, *An augmented plane wave plus local orbitals program for calculating crystal properties* (Techn. Universität Wien, Austria, 2001).